Composite Structures 134 (2015) 95–105

Contents lists available at ScienceDirect

Composite Structures

journal homepage: www.elsevier.com/locate/compstruct

Experimental and numerical approaches for structural assessment in new footbridge designs (SFRSCC–GFPR hybrid structure)

Luis Javier Sánchez-Aparicio [a,*], Luís F. Ramos [b,1], José Sena-Cruz [b,1], Joaquim O. Barros [b,1], Belén Riveiro [c,2]

[a] Department of Land and Cartographic Engineering, University of Salamanca, High Polytechnic School of Avila, Hornos Caleros, 50, 05003 Avila, Spain
[b] ISISE, Department of Civil Engineering, University of Minho, Guimarães, Portugal
[c] Department of Material Engineering, Applied Mechanics and Construction, School of Industrial Engineering, University of Vigo, Vigo, Spain

ARTICLE INFO

Article history:
Available online 20 July 2015

Keywords:
GFRP pultruded profiles
Experimental tests
Operational Modal Analysis
Finite Element Model Updating
Damage identification
Civil structures

ABSTRACT

Within the civil engineering field, the use of the Finite Element Method has acquired a significant importance, since numerical simulations have been employed in a broad field, which encloses the design, analysis and prediction of the structural behaviour of constructions and infrastructures. Nevertheless, these mathematical simulations can only be useful if all the mechanical properties of the materials, boundary conditions and damages are properly modelled. Therefore, it is required not only experimental data (static and/or dynamic tests) to provide references parameters, but also robust calibration methods able to model damage or other special structural conditions. The present paper addresses the model calibration of a footbridge bridge tested with static loads and ambient vibrations. Damage assessment was also carried out based on a hybrid numerical procedure, which combines discrete damage functions with sets of piecewise linear damage functions. Results from the model calibration shows that the model reproduces with good accuracy the experimental behaviour of the bridge.

1. Introduction

In the last few years, new civil engineering designs have emerged in the field of the construction of footbridges, considering new materials [1,2] and constructive [3–5] solutions. Within these new materials, have received special attention the use of fiber reinforced polymer (FRP) and glass fiber reinforced polymer (GFRP), offering better resistance to environmental agents and the advantages of high stiffness-to-weight and strength-to-weight ratios when compared to conventional construction materials [6,7]. They also can be combined with traditional materials, like concrete or steel, offering particularly effective flexural properties [8–10]. These hybrid structures are particularly suitable for footbridge structures thanks to the possibility of an easy and quick erection.

However, several characteristics restrict the use of this type of materials: (i) high deformability (low elastic and shear modulus); (ii) brittle failure; (iii) behaviour at elevated temperatures; and (iv) lack of specific design codes [11]. Due to the small service loads, these structures usually are light and slender. For these reason the interaction with pedestrians or wind can arise some structural problems [12,13]. Considering the mentioned above, several tests are needed in order to assess the structural behaviour of these structures in different scenarios. The diversity of materials and the interaction between them makes the Finite Element Methods (FEM) as the most feasible solution to evaluate and simulate these structures.

In contrast with the potentialities that the FEM can offer, some choices (mechanical properties of the materials or structural conditions) may give erroneous numerical results. Within this context, this paper attempts to demonstrate a methodology to evaluate, through experimental tests and robust numerical calibration strategies, the structural behaviour of a pedestrian bridge prototype. The bridge was experimentally tested with several static and dynamic tests and with the main results, a model calibration was performed to tune the mechanical parameters.

In order to obtain a robust finite element model, which represent accurately the structural behaviour of the footbridge a

Abbreviations: GFRP, Glass Fibre Reinforced Polymer; SFRSCC, Steel Fibre Reinforced Self-Compacting Concrete; FEM, Finite Element Method; FEMU, Finite Element Model Updating; MAC, Modal Assurance Criterion.

* Corresponding author. Tel.: +34 920353500; fax: +34 920353501.
E-mail addresses: luisj@usal.es (L.J. Sánchez-Aparicio), lramos@civil.uminho.pt (L.F. Ramos), jsena@civil.uminho.pt (J. Sena-Cruz), barros@civil.uminho.pt (J.O. Barros), belenriveiro@uvigo.es (B. Riveiro).
[1] Tel.: +351 253510200; fax: +351 253510217.
[2] Tel.: +34 1 986814052; fax: +34 986811924.

http://dx.doi.org/10.1016/j.compstruct.2015.07.041
0263-8223/

damage assessment was carried out, based on an hybrid numerical procedure, which combines discrete damage functions with sets of piecewise linear functions to evaluate the damage present at the structure. Special attention was paid to the influence of the supports, the interaction between structural components and the damage response of the SFRSCC deck.

This paper is organized as follows: Section 1 is the introduction; Section 2 a general structural description of the hybrid footbridge is presented; Section 3 presents the static and dynamic tests performed on the footbridge; Section 4 a robust dynamical-static calibration process is carried out; and finally in the Section 5 the conclusion are drawn.

2. GFRP–SFRSCC hybrid footbridge

2.1. Description of the structure

The studied prototype at full scale was developed in the framework of research project PONTALUMIS – Development of a prototype of a pedestrian bridge in GFRP-ECC, involving ICIST/Instituto Superior Técnico, ISISE/University of Minho and company ALTO – Perfis Pultrudidos, Lda. The footbridge design was carried out considering the main potentialities of the used materials. Therefore, the composite Steel Fiber Reinforced Self-Compacting Concrete (SFRSCC) material was placed in zones where compressive stresses exist, whereas GFRP girders were used to carry the tensile stresses. The cross section of the bridge is characterized by the following: (i) a SFRSCC deck; (ii) SFRSCC jackets placed in the vicinity of the supports; and (iii) GFRP girders (Fig. 1).

The connection between the structural components (SFRSCC deck and GFRP pultruded girders) was made through two different solutions: (i) for the contact areas located above the jackets an epoxy resin layer with 2 mm of thickness was used; and (ii) for the remaining contact zones the same adhesive solution was used in combination with a redundant mechanical connection based on M10 stainless steel bolts, with 300 mm of spacing (two per main girder's flange), in order to extend the bridge life time due to rheological effects, vandalism and accidental loads.

Complementary to the previous structure, a group of secondary girders were placed between the main ones. This solution prevents any distortion caused by eccentric loads. Positioned at the support, quarterspan and midspan sections, this profiles were constituted by I-shaped ($200 \times 100\ mm^2$) GFRP pultruded profiles and connected to the main girders by means of equal length angle GFRP ($60 \times 8\ mm^2$) profiles and stainless steel bolts (M10) threaded rods and nuts.

The footbridge structure presents a total length of 11.00 m on two pairs of supports (two pinned and two sliding), as show (Fig. 2). More details can be found elsewhere [11].

2.2. Mechanical properties of the footbridge components

Made by E-glass fiber rovings and mats embedded in a isophthalic polyester, the main and secondary pultruded profiles have been characterized by the following tests [11]: (i) tension (EN ISO 527) [14]; (ii) compression (ASTM D 695) [15]; and (iii) shear test (10° off-axis tension test), according to the recommendations of Hodgkinson [16]. Allowing the evaluation of several material mechanical properties, namely: (i) longitudinal elasticity modulus in tension ($E_{L,t}$); (ii) transverse elasticity modulus in compression ($E_{T,c}$); (iii) in-plane shear modulus (G_{LT}); (iv) longitudinal tensile strength ($f_{tu,L}$); and (v) in-plane shear strength ($T_{u,LT}$). These properties are summarizes in Table 1.

For the SFRSCC material, a specific mixture composition was used (details about the mix design are available in [17]: (i) cement; (ii) limestone filler; (iii) water; (iv) superplasticizer; (v) fine sand; (vi) river sand; (vii) crushed stone; and (viii) fibers. The compressive strength and flexural properties of the SFRSCC were assessed according to standards NP EN 12390-3 [18] and RILEM TC 162-TDF, respectively [19], providing the following mechanical information: (i) Young's modulus; (ii) compressive strength (f_{cm}); (iii) cracking strength in flexure ($f_{ct,L}$); (iv) equivalent flexural tensile strengths ($f_{eq,2}$ and $f_{eq,3}$); and (v) residual flexural tensile strengths ($f_{R,1}$ to $f_{R,4}$) (see Table 2).

The epoxy adhesive used to bond the main girders to the SFRSCC deck has an elasticity modulus in tension of $E_a = 8.8$ GPa and a tensile strength of $f_{au} = 17.3$ MPa [20]. The redundant mechanical connection into the span between jackets was materialized by stainless steel anchors (M10 × 55). This solution present a bearing capacity of $f_{bk} = 700$ MPa (according to the manufacturer). For the present study case, three different types of connections had been considered: (i) epoxy layer; (ii) epoxy layer and bolt; and (iii) bolt L-union between secondary and main girders. This connection were materialized through interface elements, considering the mechanical properties obtained in the different experimental program carried out (Table 3).

3. Experimental programs

3.1. Static test

In order to ensure the correct erection, disposition and performance of the different structural elements in the footbridge several static tests were performed [11]. These experimental tests were mainly focused on the characterization of the bending response of the footbridge, as well as the deformation recovery after unloading. For this purpose, the footbridge was loaded with multiple close-spaced water reservoirs, with a total weight of 8.8 kN/m^2. These reservoirs were placed in different uniformly and distributed configurations (load case A–C, see Table 4). All the loading and unloading operations were performed as fast as possible in order to minimize creep effects on the concrete. As a result, three load configuration (A–C) were evaluated: (i) load distributed on the entire span with a width of 1.20 m; (ii) load in the central part of the span with a length of about 2.70 m and a small gap of 0.30 m in the vicinity of midspan; and (iii) load in the central part of the span with a length of 5.10 m and a small gap of 0.30 m in the vicinity. In order to evaluate the different load setups, different sensors were placed along the footbridge: (i) electrical transducers (with a precision of 0.01 mm); and (ii) axial strains electric strain gauges (Fig. 3).

As results of the static tests (see Table 4 and Fig. 3), the acquired data was distributed into five groups, namely: (i) midspan deflection ($\delta_{ms,Avg}$); (ii) axial strains on the SFRSCC deck ($\varepsilon_{c,Avg}$); (iii) axial strains on the web of the main girders ($\varepsilon_{w,Avg}$); (iv) axial strains on the bottom flanges of the main girders ($\varepsilon_{c,Avg}$); and (v) curvature at midspan (ζ).

3.2. Dynamical identification test

A dynamical identification campaign, based on the Operational Modal Analysis (OMA) approach, was performed with the aim of identifying the modal properties of the structure. With a sensitivity of 10 V/g, range of ±0.5 g, and 8 μg rms broadband resolution, a total of eighteen uniaxial piezoelectric accelerometers were place on different locations on the vertical direction (Fig. 4).

By using Enhanced Frequency Domain Decomposition (EFDD) technique [22] each mode is estimated as a decomposition of the system's response spectral densities into several single degree of freedom systems.

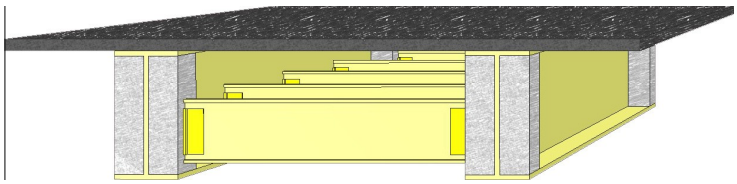

Fig. 1. Isometric view of the footbridge (in dark-grey the SFRSCC concrete, in light-grey the SFRSCC jackets and in yellow the GFRP profiles). (For interpretation of the references to colour in this figure legend, the reader is referred to the web version of this article.)

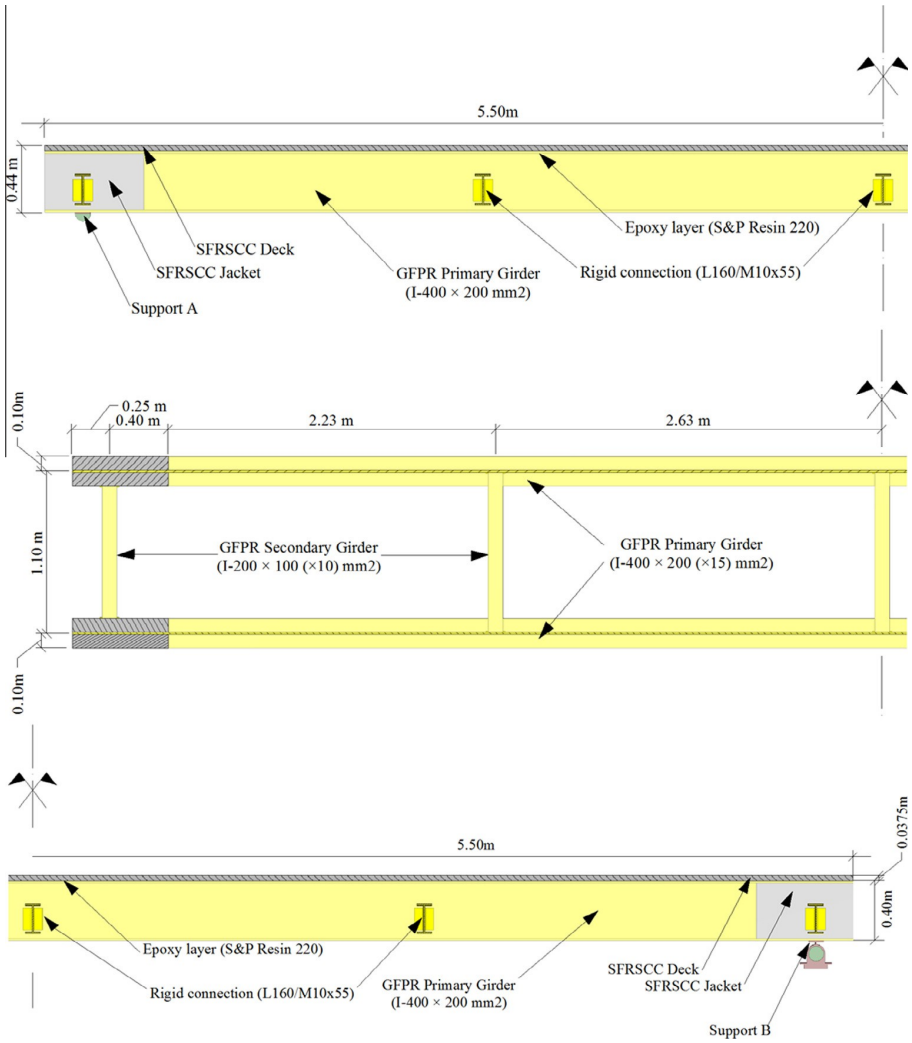

Fig. 2. Section views of the SFRSCC–GFPR footbridge (units in meters). Longitudinal sections (above and middle). Transversal view (below).

Table 1
Mechanical properties of the GFRP pultruded profiles [11].

Part	$E_{L,t}$ (GPa)	$E_{T,c}$ (GPa)	G_{LT} (GPa)	$f_{tu,L}$ (MPa)	$T_{u,LT}$ (MPa)	p (kN/m^3)
GFRP web	23.98 ± 1.61	4.55 ± 0.52	3.49 ± 0.43	278.90 ± 23.78	20.42 ± 1.15	18.00
GFRP flange	35.71 ± 1.83	3.57 ± 0.36	–	336.94 ± 37.51	–	18.00

Table 2
Mechanical properties of the SFRSCC material used [11].

$E_{c,28}$ (GPa)	f_{cm} (MPa)	$f_{ct,L}$ (MPa)	$f_{eq,2}$ (MPa)	$f_{eq,3}$ (MPa)	$f_{R,1}$ (MPa)	$f_{R,2}$ (MPa)	$f_{R,3}$ (MPa)	p (kg/m^3)
37.75 ± 1.3	75.95 ± 10.0	6.21 ± 1.2	10.42 ± 2.4	10.56 ± 2.4	10.17 ± 2.1	10.27 ± 2.34	9.71 ± 2.34	2325.78

Table 3
Mechanical properties obtained in the experimental program [21].

Variable	Epoxy layer	Epoxy layer and bolts	Bolt union
K (N/m^3) × 10^6	288.55 ± 59.75	300.57 ± 71.79	140.02 ± 9.63

A total of 16 vibration modes were identified. It is noted that, in this modal identification, several modal shapes present an asymmetric behaviour. This phenomenon can be attributed to the presence of damage in the structure especially in the first and fourth quarterspan (Fig. 5).

Following this antisymmetric behaviour in the different vibration modes, a visual inspection was carried out. Some micro-cracks on the SFRSCC deck were detected, the average value of the crack width being about 0.06 mm, in the vicinity of the quarterspans and an isolate crack in the midspan, with an average value of 1.5 mm (Fig. 6).

4. Finite element updating strategy

4.1. Numerical model of the footbridge

In order to simulate the structural (static and dynamic) behaviour of the footbridge a tridimensional FE model was built using the commercial software TNO Diana [23]. With a total of 24,334 elements high-order elements (CHX60) [23], with 10 cm as the maximum dimension (Fig. 7). For the epoxy connections (main girder-deck and secondary girder-primary girder) interfaces elements were chosen, avoiding the use of highly distorted solid elements, since the width of these connections are about 2 mm. As a result, 3,240 interface elements (Q24IF) were used.

The numerical model includes the following structural components: (i) GFRP main girders; (ii) GFRP secondary girders; (iii) bolted connections with a GFRP L union; (iv) SFRSCC deck; (v) SFRSCC jackets; (vi) epoxy-bolt layer; and (vii) epoxy layer. All the structure is supported by two groups of pinned supports (in the left side) and other two groups of sliding supports (right side). Both supports are modelled by 88 spring elements in the main directions (SP2TR).

Finally, the material properties (mean and deviation values) obtained by the different tests carried out (see Tables 1–3), were consider for the FE model. Also a perfect normal bond was assumed at the GFRP-epoxy and SFRSCC-epoxy interfaces, consider only the interface stiffness [1].

4.2. Cost function and optimization algorithm

Finite Element Model Updating (FEMU) strategy can be employed in a wide range of applications [24–26]: (i) design; (ii) simulation; (iii) prediction; and (iv) damage identification. In this context, several approaches can be carried out [27]: (i) Deterministic approaches; (ii) Bayesian finite element strategies; and (iii) Fuzzy approaches.

For the present study case, a deterministic strategy was followed. The success of this approach is based on minimizing the residual vector (r) of the objective function (J), considering the data derived from the experimental campaigns, defined by the Eq. (1).

$$r = \frac{1}{2}\left\| \begin{matrix} J^{sta} \\ J^{din} \end{matrix} \right\|^2 \tag{1}$$

where $\|\bullet\|$ denotes the Euclidean norm, r is the residual vector of J^{sta} and J^{din} (static and dynamic residuals, respectively). The objective function terms ($J = J^{sta} + J^{din}$) are given by:

$$J^{sta} = \frac{1}{2} W_\delta \sum_{j=1}^{m} \left(\frac{\delta_j^{num} - \delta_j^{exp}}{\delta_j^{exp}} \right)^2 \tag{2}$$

$$J^{din} = \frac{1}{2}\left[W_f \sum_{i=1}^{m} \left(\frac{f_i^{num} - f_i^{exp}}{f_i^{exp}} \right)^2 + W_\phi \sum_{i=1}^{m} \left(\phi_i^{num} - \frac{\phi_i^{exp}}{|\phi_{ref}^{exp}|} \right)^2 \right] \tag{3}$$

where W_f, W_φ, and W_δ are the weights considered for the frequency, vibration modes and static displacements, respectively, f is the frequency, ϕ the modal displacements, δ the static displacements, and ϕ_{ref} is a scaling factor (normalization) that enable a comparison between the experimental and numerical modes displacements. For the dynamic functions (J^{din}) the i index indicates the mode shape and for the static one (J^{sta}) the j index indicates the load case.

Generally, the residuals values (r) of the objective function (J) to be minimized shows a non-linear relation with the unknowns. For these purpose a non-linear least squares function was used to solve the problem. Inside this non-linear least squares framework the Trust Region Reflective iterative algorithm was employed. In each iteration, the search area is reduced to a zone known as "*trust region*" [28]. Finally, the objective function (J) was approximated to a quadratic minimizer by the truncated Taylor series.

As exposed in [27], the gradient-based optimizations method, in our case the Gauss–Newton approach with the Trust Region Reflective algorithm, requires the computation of the Jacobian (or sensitivity matrix) and Hessian matrix. Both matrix can be solved following a special structure integrated into the least squares problem Eqs. (4) and (5).

$$\nabla J(\theta) = \sum_{i=1}^{m} r_i(\theta) \nabla r_i(\theta) = Jacob(\theta)^T r(\theta) \tag{4}$$

$$\begin{aligned} \nabla^2 J(\theta) &= Jacob(\theta)^T Jacob(\theta) + \sum_{i=1}^{n} r_i(\theta) \nabla^2 r_i(\theta) \\ &\cong Jacob(\theta)^T Jacob(\theta) \end{aligned} \tag{5}$$

Table 4
Static test results for the three different load configurations [11].

Setup	$\delta_{ms,Avg}$ (mm)	$\varepsilon_{c,Avg}$ (μm/m)	$\varepsilon_{w,Avg}$ (μm/m)	$\varepsilon_{f,Avg}$ (μm/m)	ζ (10^{4}m^{-1})
A (along the entire span)	38.07	−190	320	1102	30.6
B (central part of the span)	23.27	−145	220	712	20.3
C (central part of the span)	43.28	−252	392	1208	34.6

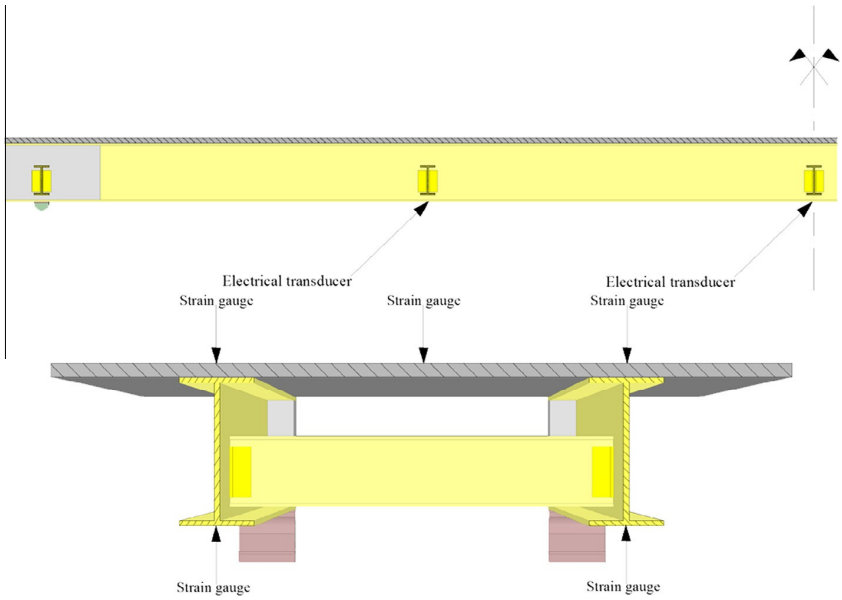

Fig. 3. Cross-section of the footbridge: Longitudinal cross-section, with the electrical transducers (above). Transversal cross-section, at mid-span, with the strain gauges sensors (below).

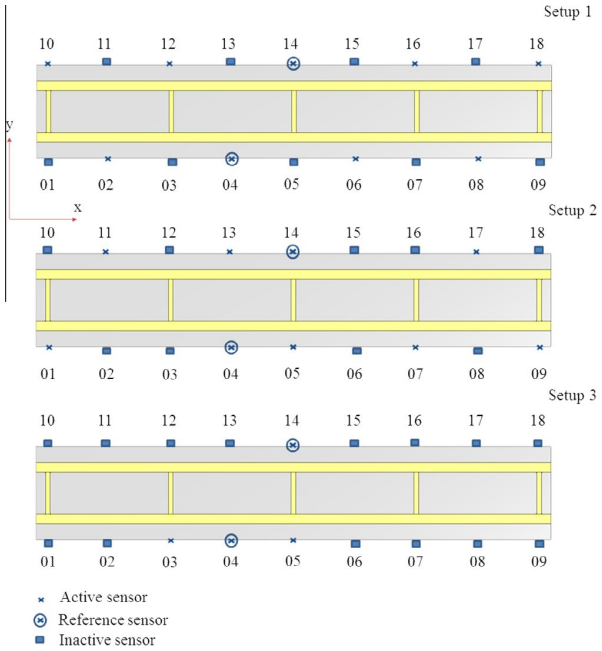

Fig. 4. Modal identification test: accelerometers positions and test setups.

where *Jacob* is the Jacobian matrix, r the vector which contains the residuals, θ the different variables that will be optimized, ∇J is the first derivate of the objective function and $\nabla^2 J$ the second one. The index n indicates the number of unknowns consider during the optimization.

Aiming at avoiding unrealistic results, boundary constraints were applied to the updating parameters, based on the deviation values obtained in the different mechanical test (see Tables 1–3) and other values provided in literature [13,20,21]. With respect to the model updating, only the first six vibration modes were considered (see Table 5).

4.3. Robust model updating

Given the complexity of the structure, several calibration stages were considered, namely: (i) initial model updating; (ii) support stiffness model updating; and (iii) damaged model updating. As model robustness indicators for results quality check, the following quantities were used: (i) relative error between frequencies; (ii) modal assurance criterion [29]; and (iii) relative error between displacements for the different load cases.

In the first stage, on the initial model updating only the Young's modulus of the main materials (SFRSCC deck, pultruded profiles flanges and webs) and the stiffness of the different epoxy solutions (with and without bolt redundancies, see Section 2.2) were calibrated (see Table 6). It should be stressed that, for the pultruded profile material and given its orthotropic behaviour, in order to reduce the number of updating variables a constant relation between longitudinal and transversal Young's modulus was

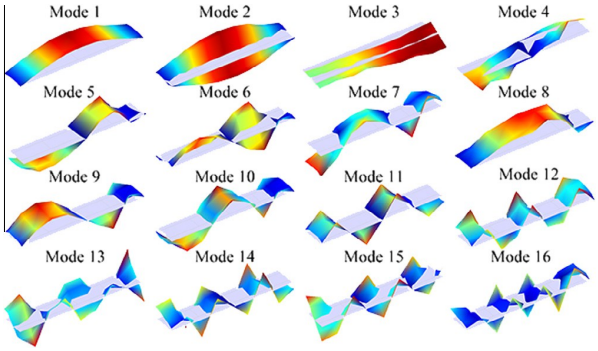

Fig. 5. Results of the 16 modes obtained from the Operational Modal Analysis campaign (the *x* axis was consider along the longitudinal direction, the *y* along the transversal and *z* along the orthogonal direction) [11].

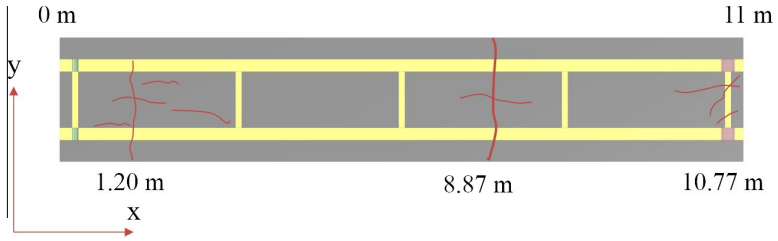

Fig. 6. Damage inspection on the footbridge (cracks are in red color). (For interpretation of the references to colour in this figure legend, the reader is referred to the web version of this article.)

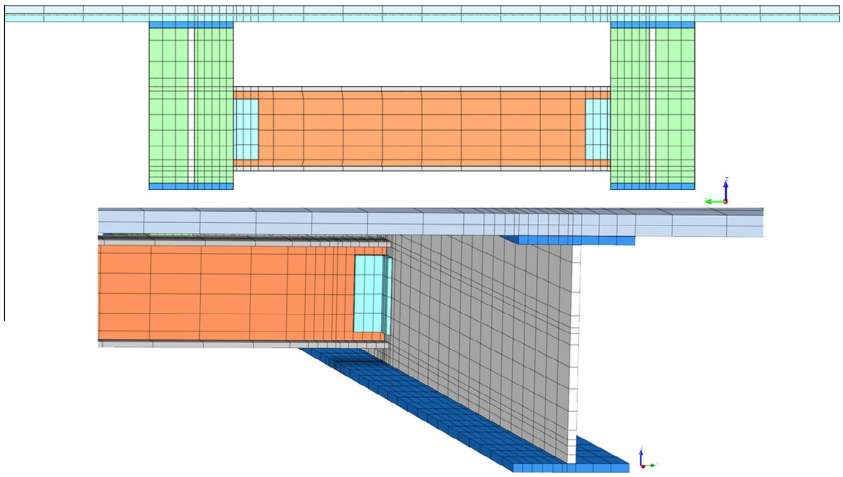

Fig. 7. Front view of the mesh model (above). Mesh detail of the inner part (below).

Table 5
Results values from the Enhanced Frequency Domain Decomposition.

Mode shape	Frequency		Damping ratio		Description
	Mean value (Hz)	CoV (%)	Mean value (Hz)	CoV (%)	
1	6.40	0.28	1.89	18.69	1st Vertical bending mode
2	8.16	0.01	1.26	11.77	1st Lateral Torsional mode
3	12.13	0.63	1.96	16.28	1st Lateral bending mode
4	20.78	12.28	1.57	62.08	2nd Torsional mode
5	22.16	6.14	0.92	20.59	2nd Vertical bending mode
6	23.74	0.09	0.76	11.65	3rd Torsional mode

Table 6
Results of the initial model robust calibration.

	Initial values	Lower bound	Upper bound	Updated values
E_{SFRSCC} (GPa)	37.75	33.82	41.68	39.90
$E_{GFRP\text{-}FLAN}$ (GPa)	35.71	30.22	41.20	41.12
$E_{GFRP\text{-}WEB}$ (GPa)	23.98	19.15	28.81	28.80
K_{EPOXY} (N/m^3)	14.43×10^{10}	5.53×10^{10}	23.33×10^{10}	17.3×10^{10}
$K_{EPOXY\text{-}BOLT}$ (N/m^3)	15.03×10^{10}	4.27×10^{10}	25.79×10^{10}	25.2×10^{10}

established ($E_{L,t}/E_{t,c}$): (i) 5.27 for the GFPR webs; and (ii) 10.00 for the GFPR flanges. This relation was considered in the different calibration procedures.

Following the results obtained in Table 4 with above considerations, the model has high static and dynamic deviations with an average error in frequencies and displacement of 33.06% and 55.04%, respectively (see Tables 7 and 8). Also, the third mode shape was not identified numerically.

Taking into account the previously results, it follows that the structural consideration of the initial model do not fit with the real behaviour of the footbridge (high structural stiffness). As a subsequent calibration, the footbridge supports were modelled with a different approach. Elastic springs in the main directions of both supports were considered, and subsequently a sensitivity analysis was performed, taking into account the initial values proposed by [13]. The results obtained in this analysis shows that the elastic springs are extremely sensitive, especially in the x and y direction. The same initial values and bounds have been considered for the elastic modulus, obtaining the presented in Table 9.

Analyzing the results obtained in terms of quality index (Figs. 8 and 9), an average relative error of 3.5% (relative error between frequencies) was obtained. Additionally, an average MAC value of

Table 7
Summary of the dynamical results obtained with the initial considerations, in terms of relative error in frequencies and MAC values.

Vibration mode	f_{exp} (Hz)	f_{num} (Hz)	Error (%)	MAC (%)
1	6.40	10.69	67.05	98
2	8.16	10.80	32.39	99
3	12.13	–	–	–
4	20.79	20.04	-3.59	82
5	22.16	25.86	16.70	89
6	23.74	27.09	14.10	88

Table 8
Summary of the results obtained in the initial model, through the static correlation values considered (relative error in displacement).

Load case	$disp_{exp}$ (mm)	$disp_{num}$ (mm)	Error (%)
A	−38.07	−16.08	−57.77
B	−23.27	−11.29	−51.50
C	−43.28	−19.10	−55.86

Table 9
Results obtained in the robust calibration of the spring model.

	Initial values	Lower bound	Upper bound	Update values
E_{SFRSCC} (GPa)	37.75	33.82	41.68	34.10
$E_{GFRP\text{-}FLAN}$ (GPa)	35.71	30.22	41.20	38.94
$E_{GFRP\text{-}WEB}$ (GPa)	23.98	19.15	28.81	28.81
E_{EPOXY} (N/mm^3)	14.43×10^{10}	5.53×10^{10}	23.33×10^{10}	9.72×10^{10}
$E_{EPOXY\text{-}BOLT}$ (N/m^3)	15.03×10^{10}	4.27×10^{10}	25.79×10^{10}	21.52×10^{10}
K_{Ax} (N/m)	10.00×10^{6}	10.00×10^{5}	10.00×10^{7}	4.37×10^{6}
K_{Ay} (N/m)	10.00×10^{5}	10.00×10^{4}	10.00×10^{6}	8.78×10^{5}
K_{Bx} (N/m)	10.00×10^{3}	10.00×10^{2}	10.00×10^{5}	1.69×10^{4}
K_{Bx} (N/m)	10.00×10^{5}	10.00×10^{4}	10.00×10^{6}	4.24×10^{5}

92.0% (with a minimum value of 86% in the sixth mode) was obtained and an average displacement relative error of 5.0%. Therefore, it can be stressed that the results obtained by the second model are more accurate compared with the previous one. But - from the obtained results (the different modal shapes and error in frequencies) it is observable that the different modes considered have negative and positive frequencies errors. Said phenomena indicates a wrong relation between stiffness of the different structural parts, and also burden the model calibration (Fig. 8).

Evaluating more in deep the different measurement points through the COMAC index (Co-ordinate Modal Assurance Criterion) [30] as a damage indicator (see Fig. 9), large discrepancies can be observed at different points (2, 9, 11 and 18), whose origin can be attributed to the structural damage (Fig. 6).

Considering the exposed above, it is expected that trough appropriate damage identification and quantification the results will improve. From the damage inspection previously showed (Fig. 6), it is possible to conclude that mainly three areas can be improved with the damage calibration (the vicinity of first and fourth quarter-spans with a generalize damage) and the third quarter-span (due to the presence of an isolate crack).

4.4. Damage function

Based on the classification defined by [31], four levels of damage assessment can be established: (i) level 1 or Detection; (ii) level 2 or Localization; (iii) level 3 or Assessment; and (iv) level 4 or Prediction of the remaining service life. The FEMU strategy allows a damage assessment up to level 3. This implies that this model-based approach is able of detecting, locating and quantifying the damage acting on the structure. Such potential is related to the understanding of damage in the structure. When the structure suffers damage it implies a degradation of the mechanical properties which can be simulated by the decrease of stiffness of the surrounding elements in the said area. The calibration of this structure, as well as the damage identification and extension, can

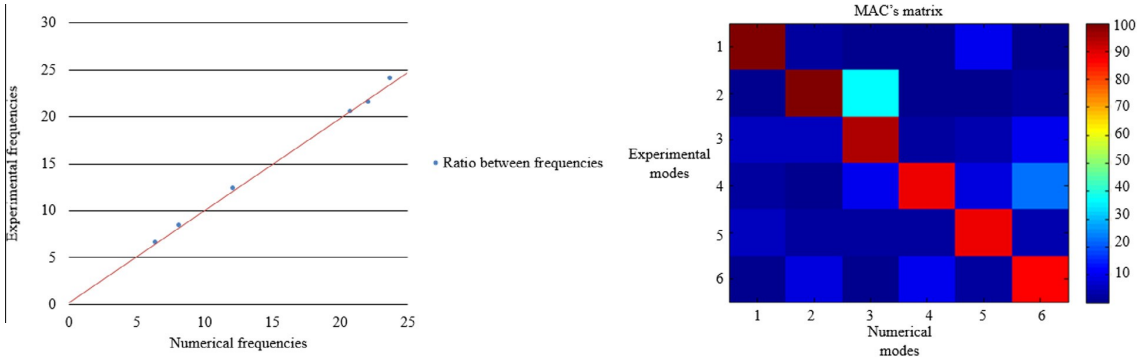

Fig. 8. Frequency pair between spring model updated and OMA (left). MAC matrix with the first six modes (right).

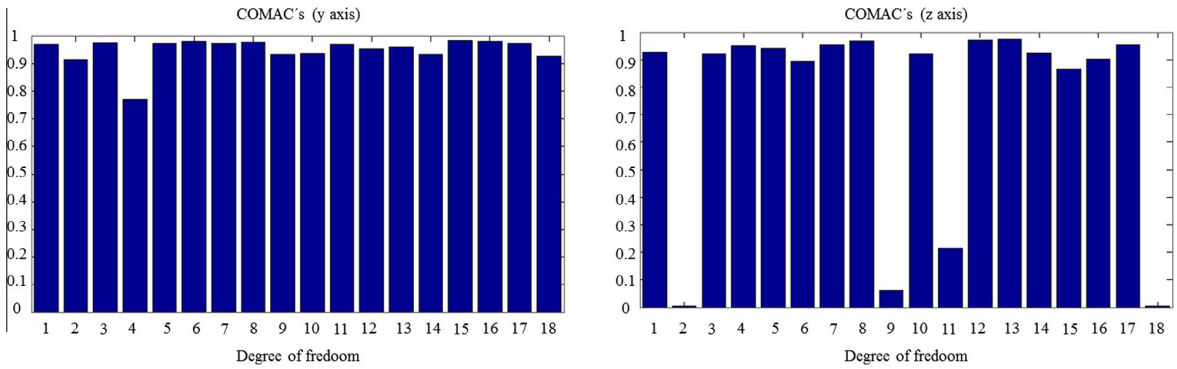

Fig. 9. COMAC values obtained in the spring model updating: COMAC values in *y* direction (left) and COMAC values in *z* direction (right).

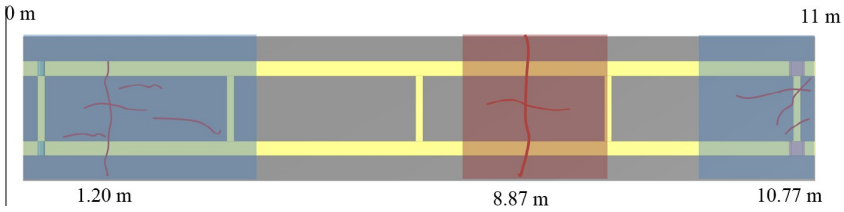

Fig. 10. Schematic representation of the damage identification strategies employed during the robust model updating. In blue the areas with substructure damage functions and in red the area with a discrete damage function. (For interpretation of the references to colour in this figure legend, the reader is referred to the web version of this article.)

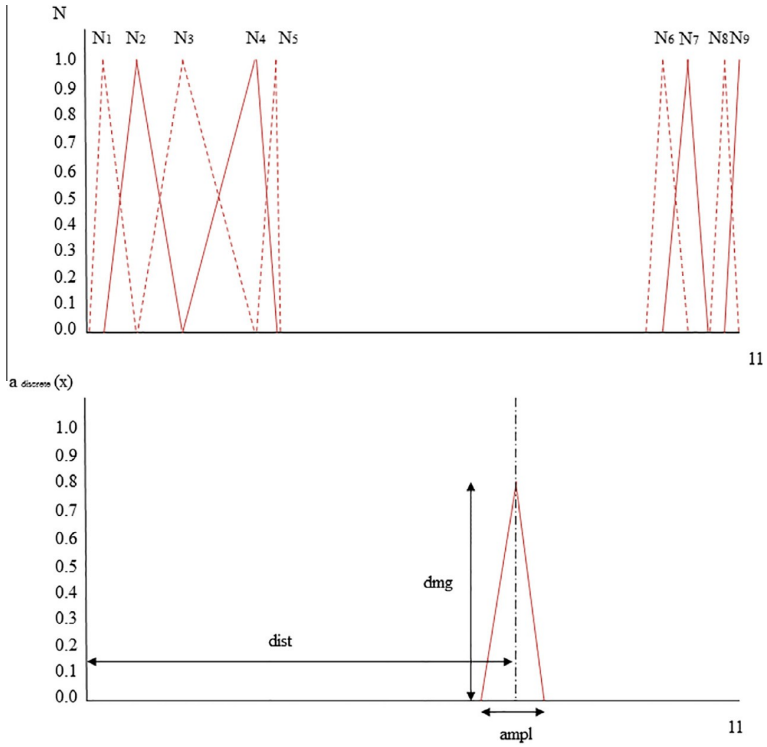

Fig. 11. Different shape functions used during the robust model updating. Substructure damage functions (above). Discrete damage function (below).

be made through the adjustment of the mechanical properties of the different elements affected by this damage.

However, adjusting the stiffness of all elements results in a large number of variables to be tuned, leading to an ill-conditioned problem that can be minimized through different approaches. One approach is the regularization technique [32]. Nevertheless, two drawbacks must be considered. On the one hand, as exposed above, evaluate the function sensitivity implies assessing the sensitivity of each variable, which results in a time consuming solution. On the other hand, less "real" results obtained by the updating of each element (non-continuous damage assumption) are obtained.

In order to solve these drawbacks, the damage quantification can be made through three different approaches: (i) discrete approach that considers the crack as a macroblock splitter through interface elements [33]; (ii) diffused approach that considers a degradation zone [25] on the surroundings of the damage area; and (iii) sub-structuring the model and applying damage functions [24,27].

Generally, the third approach could be applied successfully in different structures [32], but in contrast with the procedure showed in this updating analysis, a reference undamaged model is not available.

For these purpose, a twofold methodology was applied: (i) sensitivity analysis, maintaining the variables previously obtained, of the different damage areas through different FE bands along the damage quarter-spams; and (ii) applying a damage strategy, with different damage functions assumptions, to materialize the damage present in the structure (Fig. 10).

For the present case of study and considering the damage inspection (see Fig. 6), and the COMAC's values (see Fig. 9), an adaptation of the second and third approach was used (Fig. 10): sub-structuring technique with piecewise linear functions show in Eq. (6) for the first and fourth quarter spams (with a general damage), and a discrete damage shape function for the isolate crack shown in Eq. (7) (see Fig. 11).

Table 10
Summary of the updated variables (without consider the damage variables) obtained in the damage model calibration.

	Initial values	Lower bound	Upper bound	Update values
E_{SFRSCC} (GPa)	37.75	33.82	41.68	39.66
$E_{GFRP\text{-}FLAN}$ (GPa)	35.71	30.22	41.20	39.29
$E_{GFRP\text{-}WEB}$ (GPa)	23.98	19.15	28.81	28.81
E_{EPOXY} (N/m^2)	14.43×10^{10}	5.53×10^{10}	23.33×10^{10}	9.49×10^{10}
$E_{EPOXY\text{-}BOLT}$ (N/m^2)	15.03×10^{10}	4.27×10^{10}	25.79×10^{10}	13.13×10^{10}
K_{Ax} (N/m)	10×10^6	10×10^5	10×10^7	4.77×10^6
K_{Ay} (N/m)	10×10^5	10×10^4	10×10^6	8.98×10^5
K_{Bx} (N/m)	10×10^3	10×10^2	10×10^5	1.44×10^4
K_{Bx} (N/m)	10×10^5	10×10^4	10×10^6	4.77×10^5

$$N_{substructure,i}\begin{cases}\frac{x-x_{i-1}}{x_i-x_{i-1}} & x \in [x_{i-1}, x_i] \\ \frac{x_{i+1}-x}{x_{i+1}-x_i} & x \in [x_i, x_{i+1}] \\ 0 & otherwise\end{cases} \tag{6}$$

$$a_{discrete}(dmg, dist, ampl)\begin{cases} dmg\left(\frac{x_i - x_{dist-ampl}}{x_{dist} - x_{dist-ampl}}\right) & x \in [x_{dist-ampl}, x_{dist}] \\ dmg\left(\frac{x_{dist+ampl} - x}{x_{dist+ampl} - x_{dist}}\right) & x \in [x_{dist}, x_{dist+ampl}] \\ 0 & otherwise\end{cases} \tag{7}$$

where $N_{substructure}$ indicates the shape function for the substructure approach, x the centroid of the damage elements, x_i the border centroid between substructures, $a_{discrete}$ the damage function for the discrete approach, dmg the damage value of the function (between 0 and 1), $dist$ the distance from the origin to the point (into the discrete damage function), and $ampl$ the discrete damage aperture.

After defining the different shape functions, the damage can be applied following Eqs. (8) and (9),

$$K_{damage,i} = N_i(1 - a_i) \tag{8}$$

$$a_i = p * N_i \tag{9}$$

where $K_{damage,i}$ is the stiffness matrix which contains the damage values of the different elements affected by the damage for the shape function N_i, a_i is the damage coefficient and p is the design variables to be minimized. As a result the different values of the affected elements can ben obtained. Finally, once the different damage strategies were correctly defined, the Jacobian matrix *Jacob* needs to be re-formulated with the following considerations, Eq. (10):

Table 11
Summary of the results, for the damage model, through the dynamical correlation values considered (relative error in frequencies, MAC values).

Vibration mode	f_{exp} (Hz)	f_{num} (Hz)	Error (%)	*MAC* (%)
1	6.40	6.61	3.28	100
2	8.16	8.33	2.08	100
3	12.13	12.33	1.65	96
4	20.79	20.51	−1.35	90
5	22.16	21.52	−2.89	89
6	23.74	24.09	1.47	86

Table 12
Summary of the results obtained in the damage model, through the static correlation values considered (relative error in displacement).

Load case	$disp_{exp}$ (mm)	$disp_{num}$ (mm)	Error (%)
A	−38.07	−39.15	2.82
B	−23.27	−23.80	2.27
C	−43.28	−43.71	0.98

$$\text{Jacob}_\theta = \begin{cases} \frac{\partial J}{\partial \theta} \rightarrow \text{if } \theta \text{ is an undamage variable} \\ \frac{\partial J}{\partial \theta} = \frac{\delta J}{\delta a_{sub}} N_{sub}(\theta) \rightarrow \text{if } \theta \text{ is an substructure variable} \\ \frac{\partial J}{\partial \theta} = \frac{\delta J}{\delta a_{dis}} \left[\frac{\delta N_{dis}(\theta)}{\delta \text{dmg}} \quad \frac{\delta N_{dis}(\theta)}{\delta x_{dist}} \quad \frac{\delta N_{dis}(\theta)}{\delta ampl}\right] \\ \quad \rightarrow \text{if } \theta \text{ is an discrete variable} \end{cases} \tag{10}$$

where J is the objective function, θ variable to be updated, a and N (with the index *sub* for substructure and *dis* for discrete) the damage and shape functions and dmg, x_{dist}, $ampl$ the different variables of the discrete damage function. For the resolution of the derivatives, a finite difference approach was consider.

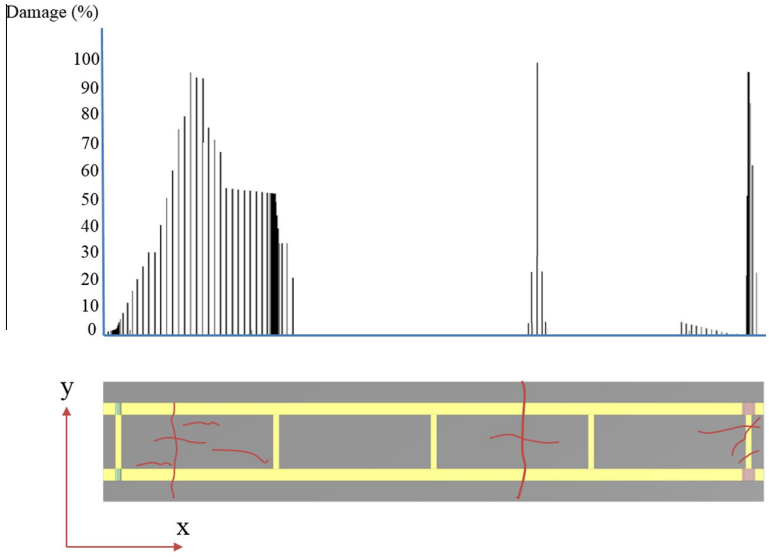

Fig. 12. Graphical comparison between the numerical and experimental damage obtained by the proposed methodology.

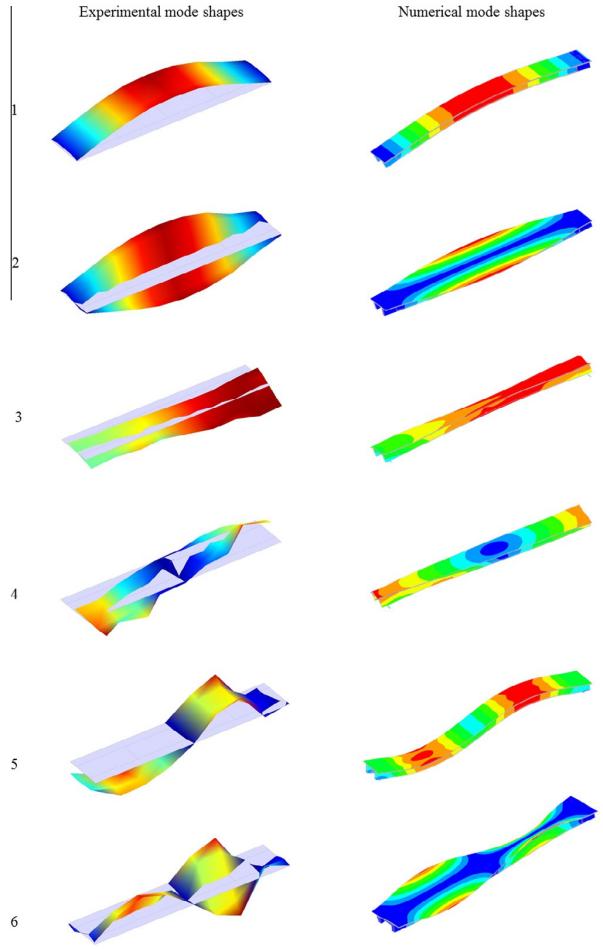

Fig. 13. Experimental and numerical mode shapes of the first six modes.

4.5. Robust calibration with damages functions

The damage presented by the footbridge can only be observed only in the intrados of the footbridge's deck. Considering this, only the lower elements of the footbridge's deck has been updated (by the proposed damage identification). As a result of the robust calibration a new model of the footbridge has been obtained (Table 10). This model presents a damage along its deck as show (Fig. 12).

Regarding the damages of the first and fourth quarterspans, as it was expected, a general damage was obtained with higher values next to the more damage areas, according with the visual inspection (Fig. 6). Also, through the discrete function, it was possible to identify the isolate crack, which is in the third quarterspan, at a distance of the deck origin equal to 7.60 m (in contrast to 7.37 m obtained in the visual inspection), originate by the presence of a transversal crack.

As a result, the final model shows a better similarity with the experimental results (see Tables 11 and 12). In terms of updating results, an average error in frequencies of 2.12% and an average MAC value of 93.50%. Considering the static behaviour, it was also observed an improvement in the results with an average error equal to 2.02%.

Finally (Fig. 13) presents a comparison between the different mode shapes identified experimentally and tuned numerically.

5. Conclusions

Nowadays, the evaluation of new constructive solutions and therefore the evaluation of new infrastructures implies a multidisciplinary task. Such analysis must involve: (i) mechanical tests of the different components; (ii) experimental programs to understand the global behaviour of the structure; and (iii) accurate numerical simulations to design, evaluate and predict its structural behaviour. Nevertheless, the interaction between different components (joints), boundary conditions and damage, are unavoidable considerations within a numerical simulation. In order to solve this, in the present paper it was shown a robust calibration method based on a non-linear least-squares method complemented by a hybrid strategy to detect and quantify the damage. The proposed methodology was validated with a high innovative structure: a hybrid footbridge based on a SFRSCC deck and GFPR pultruded profiles. The model updating analysis was carried out with results from experimental data (static and dynamic tests). It considers the stiffness of the different joints (L-union and GFPR main girders-deck union), non-perfect supports and damage as a set of linear damage functions.

Finally, an accurate damage identification analysis was performed, arising in an accurate model. However, there are always further needs of investigations in order to improve results, mainly the MAC's values for the fifth mode shape and to consider the cracks direction in the damage functions as a design variable to better improve their effects.

References

[1] Mendes P, Barros J, Sena-Cruz J, Teheri M. Influence of fatigue and aggressive exposure on GFRP girder to SFRSCC deck all-adhesive connection. Compos Struct 2014;110:152–62.
[2] Nguyen H, Mutsuyoshi H, Zatar W. Hybrid FRP-UHPFRC composite girders: part 1 – experimental and numerical approach. Compos Struct 2015;125:631–52.
[3] Bel Hadj Ali N, Rhode-Barbarigos L, Pascual Albi AA, Smith IFC. Design optimization and dynamic analysis of a tensegrity-based footbridge. Eng Struct 2010;32:3650–9.
[4] Yeh F-Y, Chang K-C, Sung Y-C, Hung H-H, Chou C-C. A novel composite bridge for emergency disaster relief: concept and verification. Compos Struct 2015;127:199–210.
[5] Chen Z, Cao H, Zhu H, Hu J, Li S. A simplified structural mechanics model for cable-truss footbridges and its implications for preliminary design. Eng Struct 2014;68:121–33.
[6] Cabral-Fonseca S, Correia JR, Rodrigues MP, Branco FA. Artificial accelerated ageing of GFRP pultruded profiles made of polyester and vinylester resins: characterisation of physical–chemical and mechanical damage. Strain 2012;48:162–73.
[7] Liao K, Schultheisz CR, Hunston DL. Effects of environmental aging on the properties of pultruded GFRP. Compos Part B Eng 1999;30:485–93.
[8] Gonilha JA, Correia JR, Branco FA. Creep response of GFRP–concrete hybrid structures: application to a footbridge prototype. Compos Part B Eng 2013;53:193–206.
[9] Keller T, Schaumann E, Vallée T. Flexural behavior of a hybrid FRP and lightweight concrete sandwich bridge deck. Compos Part A Appl Sci Manuf 2007;38:879–89.
[10] Deskovic N, Triantafillou TC, Meier U. Innovative design of FRP combined with concrete: short-term behavior. J Struct Eng 1995;121:1069–78.
[11] Gonilha J, Barros J, Correia J, Sena-Cruz J, Branco F, Ramos L, et al. Static, dynamic and creep behaviour of a full-scale GFRP-SFRSCC hybrid footbridge. Compos Struct 2014;118:496–509.
[12] Thambiratnam DP, Perera NJ, Abeysinghe CM, Huang M-H, De Silva SS. Human activity-induced vibration in slender structural systems. Struct Eng Int 2012;22:238–45.
[13] Gonilha JA, Correia JR, Branco FA. Dynamic response under pedestrian load of a GFRP–SFRSCC hybrid footbridge prototype: experimental tests and numerical simulation. Compos Struct 2013;95:453–63.
[14] ISO. ISO 527-1:2012. Plastics-determination of tensile properties. Genève. 2012.
[15] ASTM. ASTM D 695. Standard test method for compressive properties of rigid plastics. West Conshohocken, Pennsylvania. 2002.
[16] Hodgkinson JM. Mechanical testing of advanced fibre composites. Elsevier; 2000.
[17] Barros J, Pereira E, Santos S. Lightweight panels of steel fiber-reinforced self-compacting concrete. J Mater Civil Eng 2007;19:295–304.

[18] IPQ IpIQ. NP EN 12390-3:2011. Testing hardened concrete part 3: compressive strength of test specimens, Caparica; 2011.
[19] RILEM. International RILEM workshop on test and design methods for steel fibre reinforced concrete-background and experiences; 2003.
[20] Firmo JP, Correia JR, França P. Fire behaviour of reinforced concrete beams strengthened with CFRP laminates: protection systems with insulation of the anchorage zones. Compos Part B Eng 2012;43:1545–56.
[21] Gonilha J, Aquino A, Correia J, Branco F. Experimental evaluation of the GFRP/ECC connection–shear connection tests: phase 1. ICIST internal project report A. 5; 2010.
[22] Gade S, Møller N, Herlufsen H, Konstatin-Hansesn H. Frequency domain techniques for operational modal analysis. 1st IOMAC Conference; 2005.
[23] Diana T. Finite element analysis user's manual-release 9.4. 4. TNO DIANA; 2011.
[24] Teughels A, De Roeck G. Damage assessment of the Z24 bridge by FE model updating. Key engineering materials. Trans Tech Publ; 2003 [p. 19–26].
[25] Ramos LF, Marques L, Lourenço PB, De Roeck G, Campos-Costa A, Roque J. Monitoring historical masonry structures with operational modal analysis: two case studies. Mech Syst Signal Processing 2010;24:1291–305.
[26] Mishra AK, Chakraborty S. Development of a finite element model updating technique for estimation of constituent level elastic parameters of FRP plates. Appl Math Comput 2015;258:84–94.
[27] Simoen E, De Roeck G, Lombaert G. Dealing with uncertainty in model updating for damage assessment: a review. Mech Syst Signal Processing 2015;56–57:123–49.
[28] Coleman TF, Li Y. An interior trust region approach for nonlinear minimization subject to bounds. SIAM J Optim 1996;6:418–45.
[29] Allemang RJ, Brown DL. A correlation coefficient for modal vector analysis. Proceedings of the 1st international modal analysis conference. SEM, Orlando; 1982. p. 110–6.
[30] Foti D. Dynamic identification techniques to numerically detect the structural damage. Open Constr Build Tech J 2013;7:43–50.
[31] Rytter A. Vibrational based inspection of civil engineering structures: unknown; 1993.
[32] Titurus B, Friswell M. Regularization in model updating. Int J Numer Meth Eng 2008;75:440–78.
[33] Sánchez-Aparicio LJ, Riveiro B, González-Aguilera D, Ramos LF. The combination of geomatic approaches and operational modal analysis to improve calibration of finite element models: a case of study in Saint Torcato Church (Guimarães, Portugal). Constr Build Mater 2014;70:118–29.